SUPPORTING INFORMATION

Spectroscopic evidence for the two C-H-cleaving intermediates of *Aspergillus nidulans* isopenicillin *N* synthase

Esta Y. Tamanaha,[1,§] Bo Zhang,[2,§] Yisong Guo,[2] Wei-chen Chang,[2] Eric W. Barr,[1,2] Gang Xing,[1,2] Jennifer St.Clair,[1] Shengfa Ye,[3,*] Frank Neese,[3] J. Martin Bollinger, Jr.,[1,2,*] and Carsten Krebs [1,2,*]

[§]EYT and BZ both made contributions warranting primary authorship

[1]*Department of Biochemistry and Molecular Biology and* [2]*Department of Chemistry, The Pennsylvania State University, University Park, Pennsylvania 16802*

[3]*Max-Planck Institute for Chemical Energy Conversion, Mülheim a. d. Ruhr, Germany*

Materials. The pJB703 plasmid encoding *Aspergillus nidulans* isopenicillin *N* synthase was generously provided by Prof. Christopher J. Schofield (Oxford University).[1] The pET28a plasmid was obtained from Novagen (Darmstadt, Germany). DNA primers were purchased from Integrated DNA Technologies (Coraville, IA). Yeast extract and tryptone were purchased from Marcor Development Corporation (Hackensack, NJ). Isopropyl-β-D-thiogalactopyranoside (IPTG) was purchased from Biosynth International (Naperville, IL). Ethylenediaminetetraacetic acid (EDTA) disodium salt dihydrate, sodium chloride, ammonium persulfate, *N*,*N*,*N*′,*N*′-tetramethyl-ethylenediamine (TEMED), and solvents used for substrate syntheses were purchased from EMD Chemicals (Gibbstown, NJ) and used without further purification. Kanamycin, phenylmethanesulfonyl fluoride (PMSF), deoxyribonuclease I (DNase I), 3-(*N*-morpholino)propanesulfonic acid (MOPS), 3-(*N*-morpholino)propanesulfonic acid sodium salt (Na-MOPS), *N*-(2-hydroxyethyl)piperazine-*N*′-(4-butanesulfonic acid) (HEPBS), tris(hydroxymethyl)-aminomethane hydrochloride (Tris-HCl), 30% acrylamide/bis-acrylamide, ferrous ammonium sulfate hexahydrate, sodium hydroxide, formic acid, *p*-methoxybenzyl chloride, 1-hydroxybenzotriazole hydrate (HOBT), butyloxycarbonyl anhydride [$(BOC)_2O$], and tris-(2-carboxyethyl)phosphine hydrochloride (TCEP•HCl) were purchased from Sigma-Aldrich (St. Louis, MO). Magnesium chloride hexahydrate was purchased from J. T. Baker (Phillipsburg, NJ). Sodium dodecyl sulfate was purchased from Pierce Chemical (Rockford, IL). Sulfuric acid was purchased from BDH Chemicals (Poole Dorset, United Kingdom). *Escherichia coli* DH5α competent cells were purchased from Invitrogen (Grand Island, NY). *Escherichia coli* BL21(DE3) cells were purchased from Gene Choice (San Diego, CA). Ni(II)-nitrilotriacetic acid (Ni-NTA) agarose resin was purchased from Qiagen (Valencia, CA). ^{57}Fe metal was purchased from Advanced Materials and Technologies (New York, NY). δ-(L-α-aminoadipoyl)-L-cysteine-

D-valine (ACV) and δ-(L-α-aminoadipoyl)-L-3,3-[^{2}H]$_2$-cysteine-D-valine (A[d_2-C]V) were synthesized by and purchased from Bachem Holding AG (Bubendorf, Switzerland). δ-(L-α-aminoadipoyl)-L-cysteine-D-1,2,3,3,3,3',3',3'-[^{2}H]$_8$-valine (AC[d_8-V]) was synthesized according to a procedure adapted from Howard-Jones, *et al.* (see below).[2] Diphenyldiazomethane was synthesized as previously described.[3] L-α-Aminoadipic acid and *S*-benzhydryl-L-cysteine were purchased from Chem-Impex International (Wood Dale, IL). *tert*-Butanol, petroleum ether, sodium bicarbonate, potassium hydrogen sulfate, tetrahydrofuran, and *iso*-butylchloroformate were purchased from Alfa Aesar (Ward Hill, MA). Anhydrous magnesium sulfate was purchased from Spectrum (New Brunswick, NJ). Triethylamine was purchased from MP Biomedicals (Santa Ana, CA). D-1,2,3,3,3,3',3',3'-[^{2}H]$_8$-valine was purchased from C/D/N Isotopes (Pointe-Claire, Quebec). 1-Ethyl-3-(3-dimethylaminopropyl)-carbodiimide hydrochloride (EDC•HCl) and benzophenone hydrazone were purchased from Acros Organics (Fair Lawn, NJ). Trifluoroacetic acid (TFA) was purchased from Avantor Performance Materials (Phillipsburg, NJ). Anisole was purchased from TCI America (Portland, OR). Absolute ethanol was purchased from Decon Laboratories (King of Prussia, PA).

Methods for overproduction and purification of IPNS

Construction of vector and strain to over-express His_6-tagged IPNS. The plasmid pJB703,[1] which contains the full-length (993 base pairs) gene encoding *Aspergillus nidulans* isopenicillin *N* synthase (IPNS), was amplified by PCR with a forward primer (5'-GCG GCG TCC G'AA TTC ATG GGT TCA GTC AGC AAA GCC AAT GTT CC-3') containing an *Eco*R I restriction site (underlined, apostrophe where the restriction occurs) and a reverse primer (5'-GCG GCG TCC CA'A GCT TCT AGG TCT GGC CGT TCT TGT TGA TCA AAC TCA CC-3') containing a *Hin*d III restriction site (underlined, apostrophe where the restriction occurs). The amplified pJB703 DNA and pET28a, containing a T7 promoter, codons specifying an in-frame 20-amino acid affinity tag with internal His_6 motif, and a kanamycin resistance gene, were both restricted with *Eco*R I and *Hin*d III and ligated together. The pET28a-IPNS (pIPNS) ligation product was then used to transform *E. coli* DH5α cells for plasmid propagation and BL21(DE3) cells for IPNS over-expression. Two DH5α transformation products were sequenced by The Pennsylvania State University DNA Sequencing Facility and found to contain the entire IPNS coding sequence properly fused to the sequence encoding the affinity tag (see Supporting Information for entire sequence of plasmid pIPNS).

Over-expression of IPNS. Cultures of the BL21(DE3) cells containing pIPNS were grown aerobically with vigorous shaking in enriched Luria-Bertani medium (rich LB, 35 g/L tryptone, 20 g/L yeast extract, 5 g/L NaCl, pH 7.0) supplemented with 0.05 g/L kanamycin. The cells were allowed to grow at 37 °C until the optical density at 600 nm (OD_{600}) reached 0.7 - 0.9, after which time the cells were rapidly cooled on ice for 15 min. Expression of IPNS was then induced by addition of IPTG to a final concentration of 1 mM. Following induction, the cultures were

shaken at 16-20 °C for an additional 16-18 h. The cells were then harvested by centrifugation at 6,000 × *g* for 30 min. The cell pellet was flash-frozen in liquid N_2 and stored at -80 °C. A typical yield was ~14 - 17 g of wet cell paste per liter of culture.

Purification of IPNS. The frozen cell paste was resuspended in 3-5 mL/g of a pH = 7.2 buffer containing 100 mM, 5 mM imidazole, 0.25 mM PMSF, 0.1 mg/mL DNase I, and 1 mM $MgCl_2$. The cells were lysed at 4 °C by a single passage through a French pressure cell or for 20 min through a microfluidizer at 16,000 psi. The resulting lysate was centrifuged at 30,000 × *g* for 20 min. The supernatant was shaken gently with Ni-NTA resin (~ 1 mL of resin per 5 mL of clarified lysate) for 1 h. The slurry was loaded into a column and washed with 6 resin volumes of 100 mM MOPS buffer, pH 7.2, containing 5 mM imidazole. Protein was eluted off the resin by washing with 100 mM MOPS, pH 7.2, containing 250 mM imidazole. Fractions containing the desired protein, as identified by the protein's absorbance at λ_{max} = 280 nm and later confirmed by denaturing sodium dodecyl sulfate polyacrylamide gel electrophoresis (SDS-PAGE) with Coomassie staining, were pooled and dialyzed to equilibrium against 2 L of 100 mM MOPS, pH 7.2, supplemented with 10 mM EDTA. The resulting apo-protein was then dialyzed two times with 2 L of 100 mM MOPS, pH 7.2, for a minimum of 4 h each time to remove excess EDTA. Following dialysis, the protein was concentrated to ~ 5-10 mM in a YM-10 centrifugal concentrator with 10,000 molecular weight cutoff filter (Merck Millipore, Billerica, MA), flash frozen by immersion in liquid N_2, and stored at –80 °C.

Determination of IPNS concentration. The concentration of apo-IPNS was determined from the absorbance at 280 nm by assuming the molar absorptivity (ε_{280} = 57.54 $mM^{-1}cm^{-1}$) calculated according to the method of Gill and von Hippel.[4]

Verification of IPNS activity. The ability of His_6-tagged *A. nidulans* IPNS to convert the substrate, ACV, to the product, IPN, was verified by exposing an anaerobic solution of the reactant IPNS•Fe(II)•ACV complex (final concentrations: 10 μM IPNS, 100 μM Fe(II), and 1mM ACV in 100 mM MOPS, pH 7.2) to ambient atmosphere for 1 h on ice (the solution was mixed every 10 min and exposed to the atmosphere to ensure adequate availability of O_2). After 1 hour, the reaction was terminated by heating at 90-100 °C for 10 min, and the quenched sample was centrifuged at 14,000 × *g*. The supernatant was then filtered through a 3,000 molecular weight cutoff (MWCO) Amicon Ultra centrifugal filter (Millipore, Billerica, MA). The filtered product was concentrated in a Savant SPD131DDA SpeedVac Concentrator (Thermo Scientific Corp., Asheville, NC) and either analyzed directly by liquid chromatography/mass spectrometry (LC/MS) or stored for no longer than overnight at -20 °C prior to analysis. For LC/MS analysis, the samples were prepared in 30% methanol, 0.05% formic acid and analyzed for ACV (*m/z* = 364, $M+H^+$) and IPN (*m/z* = 360, $M+H^+$) using a Waters Micromass ZQ liquid chromatography/mass spectrometer (Milford, MA) fitted with a 4.6 mm × 75 mm Waters Symmetry C-18 3.5 μm column. The LC/MS was tuned for ACV in the positive electrospray ionization (ESI^+) mode. The parameters were: 4.00 kV capillary voltage, 35 V cone voltage, 2 V extractor voltage, 0 V RF lens voltage, 80 °C source temperature, 350 °C desolvation temperature, 500 L/h desolvation gas flow, 100 L/h cone gas flow. The column was developed under isocratic flow of 30% methanol and 0.05% formic acid at 0.1 mL/min. The results revealed

that reconstituted IPNS converts ACV to IPN (Figure S1).

Nucleotide sequence of plasmid IPNSpET28a.

The sequence encoding IPNS from *Aspergillus nidulans* is highlighted in red below:

AAATTGCCTCTAGAATAATTTTGTTTAACTTTAAGAAGGAGATATACCATGGGCAGCAGCCATC
ATCATCATCATCACAGCAGCGGCCTGGTGCCGCGCGGCAGCCATATGGCTAGCATGACTGGTGG
ACAGCAAATGGGTCGCGGATCCGAATTCATGGGTTCAGTCAGCAAAGCCAATGTTCCAAAGATC
GATGTTTCTCCCCTGTTTGGAGACGACCAAGCAGCCAAAATGAGAGTAGCCCAGCAAATCGACG
CCGCTTCGCGTGATACTGGGTTTTTCTACGCCGTCAACCATGGGATCAATGTGCAGCGACTCTC
GCAGAAGACCAAGGAGTTTCATATGTCTATCACACCTGAGGAAAAGTGGGACCTTGCGATTCGT
GCCTACAACAAAGAGCACCAGGACCAAGTCCGTGCCGGATACTACCTGTCCATCCCCGGGAAAA
AGGCAGTCGAGTCCTTCTGCTACCTTAACCCGAACTTCACGCCCGATCATCCCCGTATCCAGGC
CAAGACTCCCACTCACGAGGTAAACGTGTGGCCAGACGAGACCAAGCACCCTGGTTTCCAAGAC
TTTGCCGAGCAGTATTACTGGGATGTTTTCGGTCTCTCTTCTGCACTGCTCAAGGGCTACGCCT
TGGCATTAGGCAAAGAGGAGAATTTCTTCGCTCGCCACTTCAAGCCAGACGATACTCTTGCCTC
GGTTGTGCTGATCCGCTACCCTTACCTGGATCCCTACCCCGAGGCTGCTATCAAGACGGCGGCC
GACGGCACCAAACTGAGTTTTGAGTGGCATGAGGATGTATCCCTAATCACTGTGCTTTACCAGT
CCAACGTGCAGAACCTGCAGGTAGAAACTGCTGCCGGGTATCAAGATATCGAGGCCGACGATAC
TGGCTACTTGATCAACTGCGGCAGTTACATGGCACATCTCACAAACAACTACTATAAAGCGCCC
ATCCATCGGGTGAAATGGGTTAATGCAGAGCGCCAGTCCCTGCCATTCTTCGTCAACCTGGGAT
ACGACAGCGTGATTGATCCATTTGATCCCCGAGAACCCAATGGCAAGTCTGATCGGGAGCCACT
CTCCTACGGCGACTATTTGCAAAACGGGCTGGTGAGTTTGATCAACAAGAACGGCCAGACCTAG
AAGCTTGCGGCCGCACTCGAGCACCACCACCACCACCACTGAGATCCGGCTGCTAACAAAGCCC
GAAAG

Synthesis of δ-(L-α-aminoadipoyl)-L-cysteine-D-2,3,4,4,4,4',4',4'-[^{2}H]$_8$-valine (AC[d_8-V])

AC[d_8-V] was synthesized in five steps according to Scheme S1 . The synthesis was adapted from the procedure used to prepare the substrate analog, δ-(L-α-aminoadipoyl)-L-cysteine-D-β-fluoro-valine.[2]

*Synthesis of N-tert-butyloxycarbonyl-L-α-aminoadipic acid (**1**)*. L-α-aminoadipic acid (2.04 g, 12.7 mmol), *tert*-butanol (17 mL), and butyloxycarbonyl anhydride $(BOC)_2O$ (10.9 g, 51.3 mmol) were added to an aqueous sodium hydroxide solution (1.07 M, 25 mL) at room temperature. The reaction mixture was then stirred for 21 h while the pH was maintained at ~10 by periodic addition of 3 N aqueous sodium hydroxide. During the course of the reaction, a dark brown solid substance coated the surface of the flask. The reaction mixture was filtered through Whatman paper (Grade 1, 11 μm particle retention size) and washed with petroleum ether (5 × 25 mL). Each layer was separated and combined with like phases from subsequent washes. The combined organic phases were extracted with an aqueous sodium bicarbonate solution (45 mL). The combined aqueous layers were acidified to pH < 3 by slow addition of potassium hydrogen sulfate at 0 °C. The resulting solution was then extracted with ethyl acetate (4 × 45 mL). The combined organic layers were washed with water (55 mL) followed by brine (55 mL), and were then dried over anhydrous magnesium sulfate. The solvent was removed under vacuum with a rotary evaporator. The remaining white solid was *N-tert*-butyloxycarbonyl-L-α-aminoadipic acid (**1**) (1.94 g, 7.4 mmol). ^{1}H-NMR (360 MHz, d_6-acetone, Figure S2): 6.23 (doublet, J = 9.0 Hz, 1H), 4.26-4.15 (multiplet, 1H), 2.38 (triplet, J = 7.0 Hz, 2H), 1.96-1.88 (multiplet, 1H), 1.85-1.70 (multiplet, 3H), 1.43 (singlet, 9H); ^{13}C-NMR (90 MHz, d_6-acetone): 173.9, 173.7 (2 × $\underline{C}O_2H$), 156.0 (*t*BuO$\underline{C}$O), 78.7 ($\underline{C}(CH_3)_3$), 53.5 (C_α), 33.1 (C_δ), 31.5 (C_β), 28.1 (C($\underline{C}H_3)_3$), 21.5 (C_γ); MS: m/z = 260 (M^-).

*Synthesis of N-tert-butyloxycarbonyl-L-α-aminoadipic acid α-p-methoxybenzyl ester (**2**)*. To *N-tert*-butyloxycarbonyl-L-α-aminoadipic acid (1.94 g, 7.4 mmol) dissolved in dimethylformamide (DMF, 19 mL, triethylamine (1.2 mL, 8.5 mmol) was added [this is messed up both linguistically and structurally], followed by *p*-methyoxybenzyl chloride (PMBCl) (1.1 mL, 8.0 mmol). The solution was stirred under argon at 38 °C for 25 hr. After the reaction, the solvent was removed under vacuum with a rotary evaporator. The resulting crude product was dissolved in ethyl acetate (30 mL) then washed with water (3 × 15 mL) and brine (15 mL). The organic phase was then dried over anhydrous magnesium sulfate, and the solvent was removed under vacuum to give *N-tert*-butyloxycarbonyl-L-α-aminoadipic acid α-*p*-methoxybenzyl ester (**2**) (2.26 g, 6.2 mmol) as a clear colorless oil. ^{1}H-NMR (360 MHz, $CDCl_3$, Figure S3): 7.32 (doublet, 2H, J = 9.0 Hz), 6.89 (doublet, 2H, J = 9.0 Hz), 5.18-5.03 (multiplet, 3H), 4.40-4.27 (multiplet,1H), 3.82 (singlet, 3H), 2.45-2.32 (multiplet, 2H), 1.92-1.63 (multiplet, 4H), 1.46 (singlet, 9H); MS: m/z = 380 (M^-).

*Synthesis of N-tert-butyloxycarbonyl-α-p-methoxybenzyl-δ-(L-α-aminoadipoyl)-S-benzhydryl-L-cysteine (**3**)*. Triethylamine was added at room temperature to a solution of *N-tert*-butyloxycarbonyl-L-α-aminoadipic acid α-*p*-methoxybenzyl ester (2.26 g, 6.2 mmol) in tetrahydrofuran (THF, 23 mL), triethylamine (0.9 mL, 6.1 mmol). After the addition was complete, the resulting solution was chilled in a NaCl/ice bath (-20 °C) and stirred for 10 min. Ice-chilled *iso*-butylchloroformate (0.8 mL, 5.9 mmol) in THF (18 mL) was then added to the reaction mixture. The resulting cloudy solution was allowed to warm to -12 °C over a period of 35 min. An ice-chilled solution of *S*-benzhydryl-L-cysteine (1.77 g, 6.2 mmol) and triethylamine (2.2 mL, 15.8 mmol) in water (23 mL) was added to the reaction solution, which was then allowed to warm to room temperature over 1.5 hr. The reaction was quenched by addition of 50

mL water, and the resulting cloudy solution was first washed with diethyl ether (3 × 50 mL) and then acidified with 6N hydrochloric acid to pH ~1. The acidic solution was then extracted with ethyl acetate (4 × 50 mL), and the combined organic extracts were washed with brine (60 mL) and dried over magnesium sulfate. The solvent was removed under vacuum with a rotary evaporator to afford a white crystalline solid, *N-tert*-butyloxycarbonyl-α-*p*-methoxybenzyl-δ-(L-α-aminoadipoyl)-*S*-benzhydryl-L-cysteine (**3**, 3.08 g, 4.9 mol).; ^{1}H-NMR (360 MHz, $CDCl_3$, Figure S4): 7.39 (doublet, J = 7.5 Hz, 2H), 7.35-7.19 (multiplet, 10H), 6.86 (doublet, J = 8.0 Hz, 2H), 6.52 (doublet, J = 7.5 Hz, 1H), 5.25 (doublet, J = 8.5 Hz, 1H), 5.21 (singlet, 1H), 5.09-5.03 (multiplet, 2H), 4.64-4.61 (multiplet, 1H), 4.34-4.29 (multiplet,1H), 3.79 (singlet, 3H), 2.89-2.78 (multiplet, 2H), 2.24-2.13 (multiplet, 2H), 1.84-1.80 (multiplet, 1H), 1.70-1.57 (multiplet, 3H), 1.41 (singlet, 9H); MS: m/z = 649 (M^-).

*Synthesis of N-tert-butyloxycarbonyl-α-p-methoxybenzyl-δ-(L-α-aminoadipoyl)-S-benzhydryl-L-cysteine-D-2,3,4,4,4,4',4',4'-[^{2}H]$_8$-valine-benzhydryl ester (**4**)*. 1-Ethyl-3-(3-dimethylaminopropyl)- carbodiimide hydrochloride (EDC•HCl), (26.3 mg, 0.14 mmol), and 1-hydroxybenzotriazole hydrate (HOBT, 18.5 mg, 0.14 mmol) in dichloromethane (DCM, 7 mL), triethylamine (37 μL, 0.28 mmol) were added to a solution of *N-tert*-butyloxycarbonyl-α-*p*-methoxybenzyl-δ-(L-α-aminoadipoyl)-*S*-benzhydryl-L-cysteine (109.5 mg, 0.168 mmol), D-2,3,4,4,4,4',4',4'-[^{2}H]$_8$-valine benzhydryl ester tosylate salt (64 mg, 0.14 mmol, synthesized according to a reported procedure from Howard-Jones, *et al*.;[2] see Figure S5 for ^{1}H-NMR spectrum) and the solution was allowed to stir at room temperature for 22 hr. After addition of 20 mL of DCM, the resulting solution was then washed with water (10 mL), aqueous hydrochloric acid (1 N, 10 mL), and water (10 mL). The solvent was removed under vacuum with a rotary evaporator. The resulting residue was dissolved in ethyl acetate (30 mL) and then washed with

saturated sodium bicarbonate (15 mL), water (15 mL), and brine (15 mL). The organic layer was dried over anhydrous magnesium sulfate, and the combined solvent was removed under vacuum. The resulting clear oil was *N-tert*-butyloxycarbonyl-α-*p*-methoxybenzyl-δ-(L-α-aminoadipoyl)-*S*-benzhydryl-L-cysteine-D-2,3,4,4,4,4',4',4'-[^{2}H]$_8$-valine benzyl ester (84 mg, 0.09 mmol). ^{1}H-NMR (360 MHz, $CDCl_3$, Figure S6): 7.45-7.20 (multiplet, 22H), 6.92 (singlet , 2H), 6.90-6.85 (multiplet, 3H), 6.11 (doublet, J = 7.5 Hz, 1H), 5.25 (singlet, 1H), 5.13 (doublet, J = 8.0 Hz, 1H), 5.08 (singlet, 2H), 4.49 (doublet, J = 7.0, 1H), 4.27-4.23 (multiplet, 1H), 3.78 (singlet, 3H), 2.80 (multiplet, 1H), 2.71 (multiplet, 1H), 2.14-2.03 (multiplet, 2H), 1.81-1.77 (multiplet, 1H), 1.64-1.55 (multiplet, 3H), 1.42 (singlet, 9H); MS: m/z = 924 (ES^+).

*Synthesis of δ-(L-α-aminoadipoyl)-L-cysteine-D-2,3,4,4,4,4',4',4'-[^{2}H]$_8$-valine (AC[d$_8$-V]) (**5**)*. *N-tert*-Butyloxycarbonyl-α-*p*-methoxybenzyl-δ-(L-α-aminoadipoyl)-*S*-benzhydryl-L-cysteine-D-2,3,4,4,4,4',4',4'-[^{2}H]$_8$-valine benzhydryl ester (84 mg, 91 μmol) was dissolved in degassed trifluoroacetic acid (3.6 mL) and degassed anhydrous anisole (220 μL, 2.0 mmol). The solution was then stirred at room temperature for 1 hr. Diethyl ether (Et_2O, 9 mL) and water (9 mL) were then added to the solution, and the Et_2O layer was extracted with water (3 × 9 mL). The combined aqueous layers were then washed with Et_2O (9 mL). The aqueous layer was then removed under vacuum with a rotary evaporator. The resulting white solid was δ-(L-α-aminoadipoyl)-L-cysteine-D-1,2,3,3,3,3',3',3'-[^{2}H]$_8$-valine (29.2 mg, 78.7 μmol). ^{1}H-NMR (300 MHz, D_2O, Figure S7): 4.49 (doublet, J = 7.0, 1H), 3.70 (multiplet, 1H), 2.90-2.66 (multiplet, 2H), 2.41-2.15 (multiplet, 2H), 1.89 (multiplet, 2H), 1.67 (multiplet, 2H); MS: m/z = 372 (ES^+).

Characterization of the Fe(IV) intermediate by variable-field Mössbauer spectroscopy

The Fe(IV) complex was further characterized by its Mössbauer spectra at 4.2 K in variable externally applied magnetic fields. A sample with the maximum quantity of the Fe(IV) complex was used. Derived spectra of the Fe(IV) intermediate were obtained by removing the appropriate contribution (determined from the zero-field spectra) of the experimental spectrum of the IPNS•Fe(II) complex collected under identical conditions from the spectrum of the sample containing the intermediate (Figure S11). These experimentally-derived "reference" spectra (Figure 3, vertical bars) can be simulated (Figure 3, red lines) according to the commonly used spin-Hamiltonian formalism (see Materials and Methods) in the slow relaxation regime with the parameters shown in the legend of Figure 3 and Table 1. The simulation reveals a large positive ZFS parameter (D = 10 cm^{-1}), which indicates that the splitting observed in the spectra reflects the internal magnetic hyperfine field in the xy plane ($B_{\mathrm{int,i}} = -\langle S_i \rangle A_i / g_n \beta_n$, i = x, y) defined by the coordinate frame of the ZFS tensor (see eq. 3). For Fe(IV)-oxo intermediates, the xy-plane is usually perpendicular to the Fe-oxo bond.[5,6] The large magnetic splitting observed in the 8-T spectrum is incompatible with the intermediate spin (S = 1) configuration but consistent with the high-spin (S = 2) configuration.[7-9] The magnitude of the splitting can be reproduced with $A_x \approx A_y \approx$ -20 MHz, values similar to those of other MNH-Fe(II) enzyme ferryl intermediates. Furthermore, the spectral simulation reveals that the sign of the quadrupole splitting parameter is negative (ΔE_Q = -0.44 mm/s), as is observed for other high-spin ferryl complexes.[10] However, simulation of the detailed spectral features, especially the unusual breadth of the splitting of the left-most line in the 8-T spectrum requires introduction of significant anisotropy of the internal magnetic field in the xy-plane. Analysis of the field-dependent spectra reveals that the anisotropy of the internal field is due to anisotropy of the hyperfine tensor (i.e. $A_x \neq A_y$) *and* anisotropy of

the spin expectation value (i.e., $\langle S_x \rangle \neq \langle S_y \rangle$). The anisotropy of $\langle \mathbf{S} \rangle$ is caused by the significant rhombicity ($E/D = 0.09$) of the $S = 2$ ground state. The rather sharp outer lines observed in the 4-T spectrum suggest a nearly isotropic internal magnetic field in the xy-plane. This observation can be rationalized by the fact that, at 4 T, the anisotropies in the xy-plane of $\langle \mathbf{S} \rangle$ and **A** cancel, resulting in a (nearly) isotropic internal field in the xy plane at that field. We further note that A_z cannot be determined at 4.2 K, due to the small spin-expectation value along the z direction, $\langle S_z \rangle$, up to 8 T. Therefore, we fixed A_z value at -41 MHz, a value similar to that experimentally observed and computationally predicted for the ferryl intermediate in taurine:2OG dioxygenase (TauD).[6] While enzyme MNH ferryl intermediates typically have (nearly) axial ZFS and hyperfine tensors, these tensors exhibit significant anisotropy for the IPNS ferryl complex. The anisotropy in **A** is reproduced by density functional theory (DFT) calculations (see below) and attributed to the unique *cis*-thiolate ligand to the cofactor in IPNS.

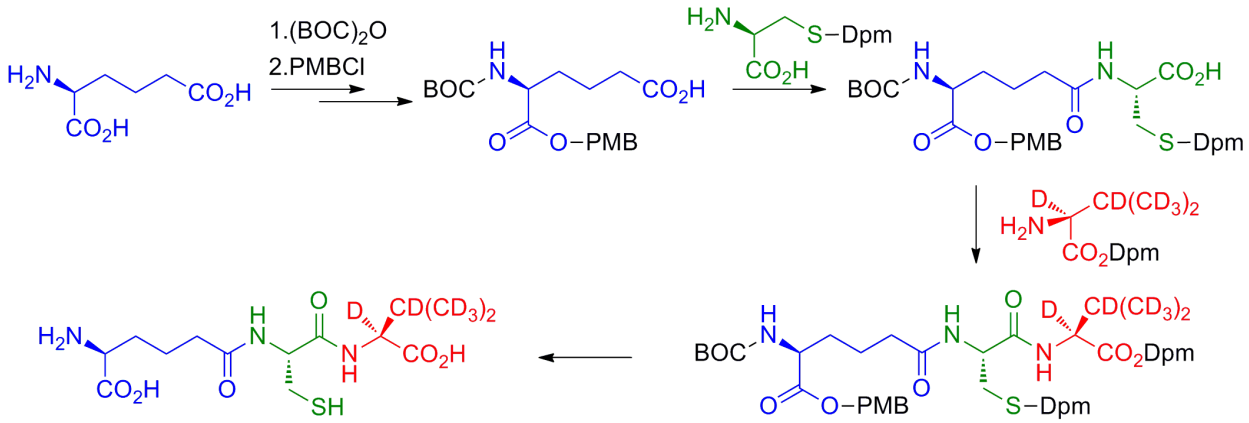

Scheme S1: Synthetic scheme used to prepare the substrate isotopolog δ-(L-α-aminoadipoyl)-L-cysteine-D-2,3,4,4,4,4',4',4'-[^{2}H]$_8$-valine (AC[d_8-V]). Experimental details for each of the steps are provided above.

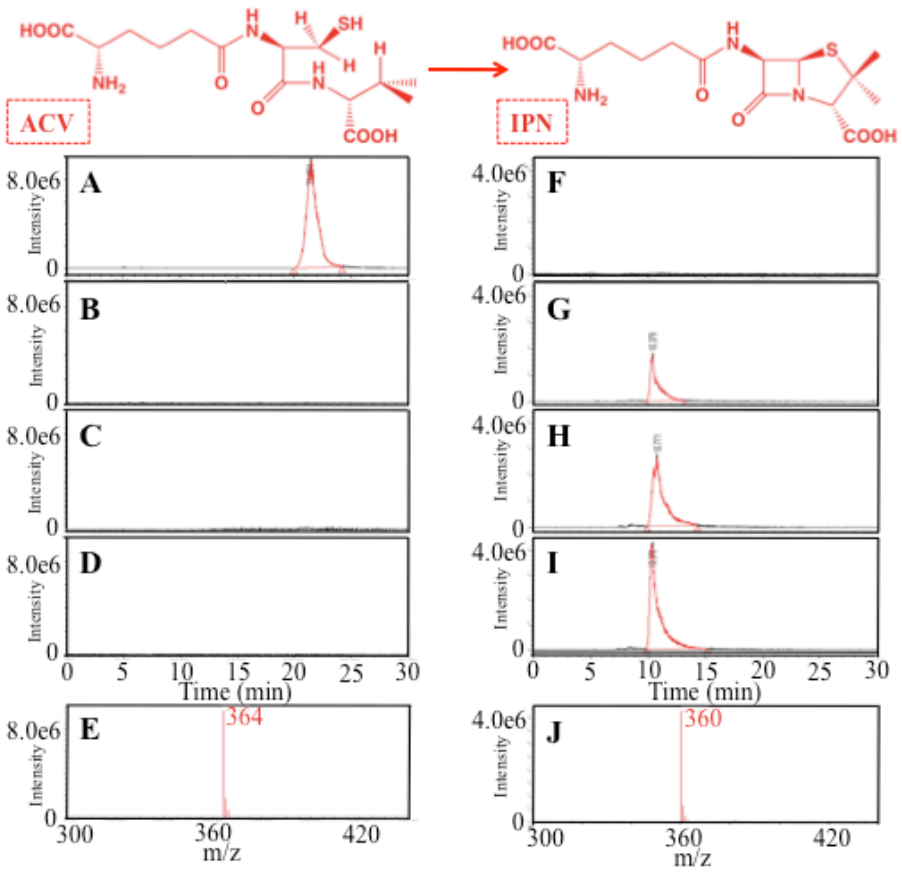

Figure S1. LC/MS analysis showing ACV consumption and IPN formation catalyzed by preparations of the recombinant IPNS. Frames **A**-**D** show single-ion *m/z* = 364 chromatograms revealing residual ACV after 1 h reactions (at 5 °C) under the conditions given below at varying ACV concentrations, and frames **F**-**J** show the corresponding *m/z* = 360 chromatograms revealing IPN produced in the same reactions. (**A** and **F**) Negative control (IPNS treated with 2% TCA prior to 1.5 mM ACV addition), (**B** and **G**) 0.5 mM ACV, (**C** and **H**) 1.0 mM ACV, (**D** and **I**) 1.5 mM ACV. (**E** and **J**) are the mass spectra of the ACV peak (retention time: 21.5 min) and the IPN peak (retention time: 10.4 min). Assay conditions: 0.2 mM IPNS, 0.3 mM Fe(II) and the indicated concentration of ACV in 100 mM HEPBS, pH 8.3. Reactions were stirred every 10 min. After 1 h, they were quenched with 2% TCA, filtered through a 3,000 kDa MWCO filter, and then completely dried. The sample was redissolved in the LC/MS mobile phase (30% methanol, 0.05% formic acid).

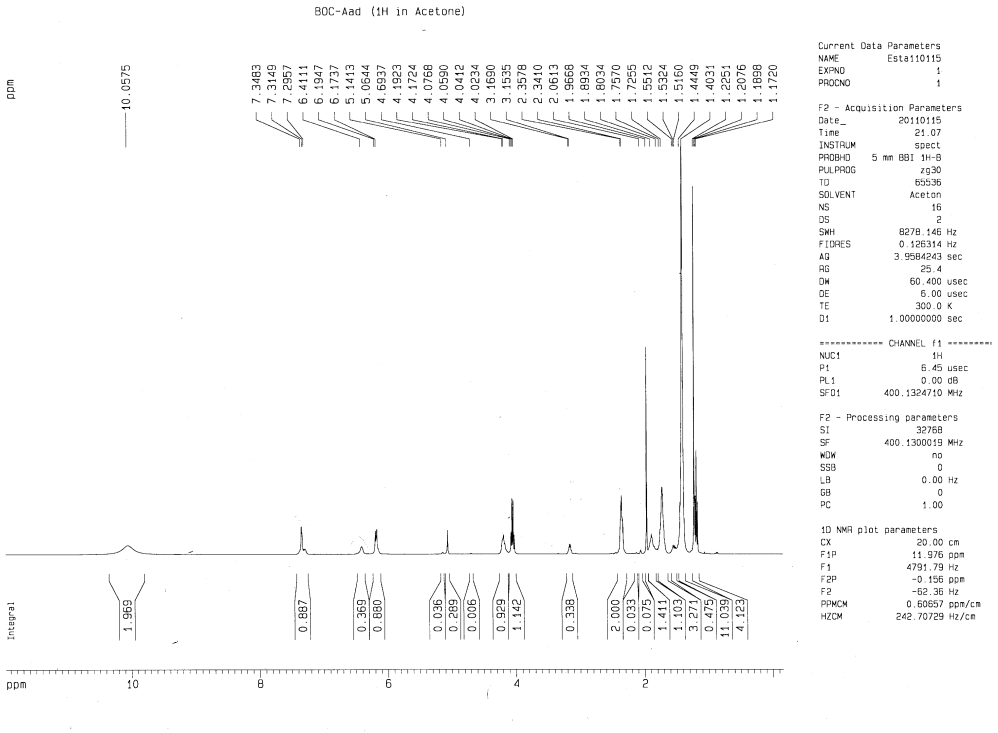

Figure S2. ^{1}H-NMR spectrum (400 MHz, 22 °C) in acetone-d_6 of *N*-*tert*-butyloxycarbonyl-L-α-aminoadipic acid.

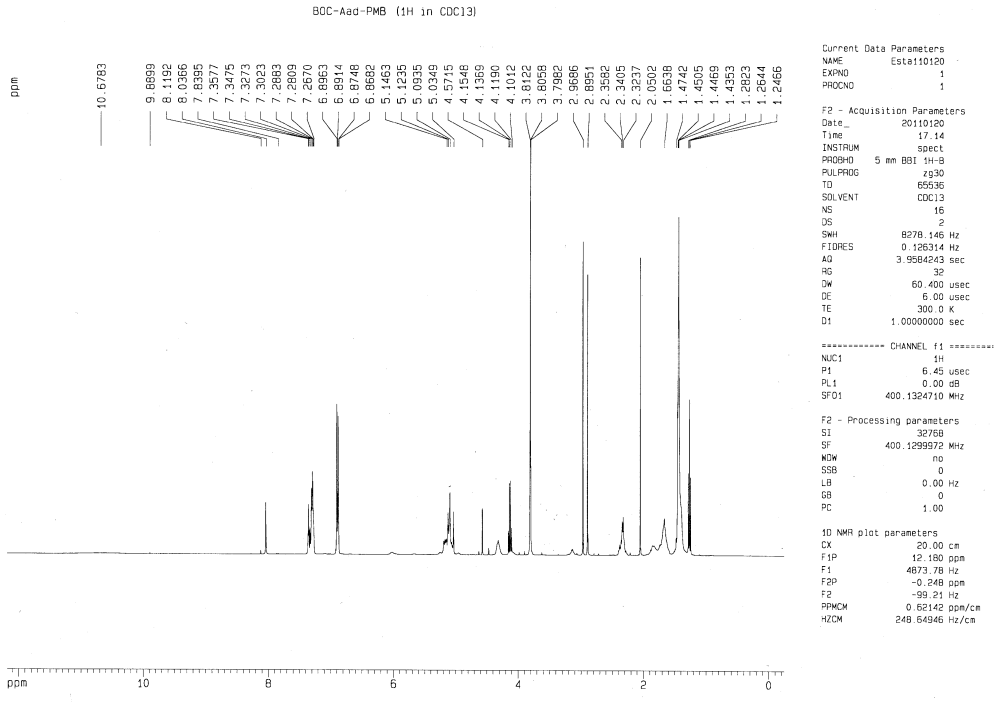

Figure S3. ^{1}H-NMR spectrum (400 MHz, 22 °C) in $CDCl_3$ of *N-tert*-butyloxycarbonyl-L-α-aminoadipic acid α-*p*-methoxybenzyl ester.

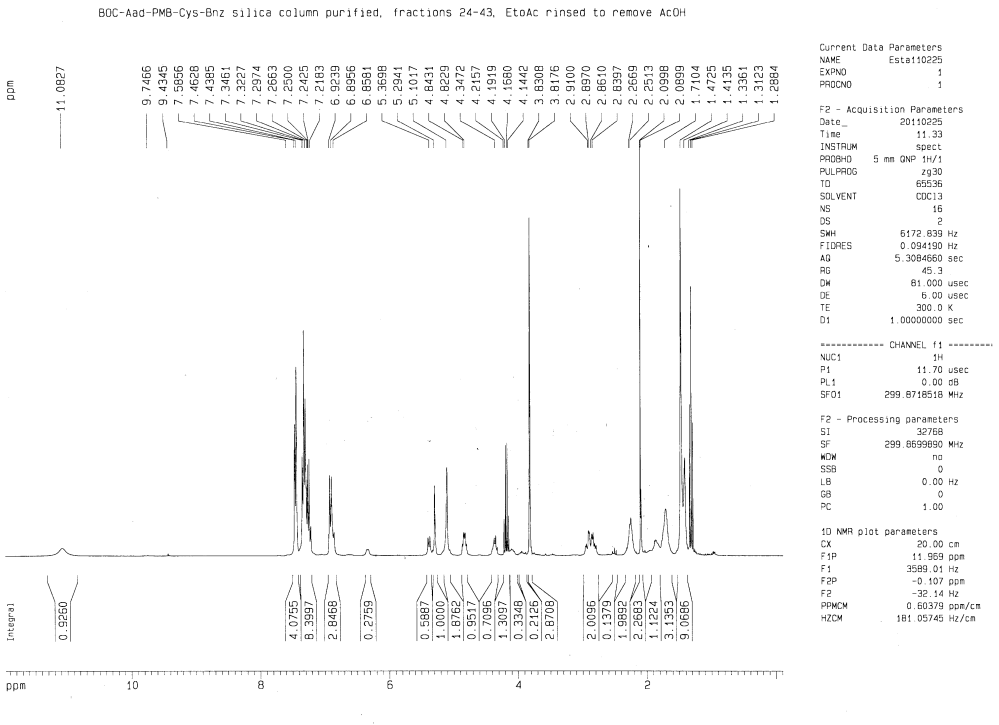

Figure S4. ^{1}H-NMR spectrum (300 MHz, 22 °C) in $CDCl_3$ of *N-tert*-butyloxycarbonyl-α-*p*-methoxybenzyl-δ-(L-α-aminoadipoyl)-*S*-benzhydryl-L-cysteine.

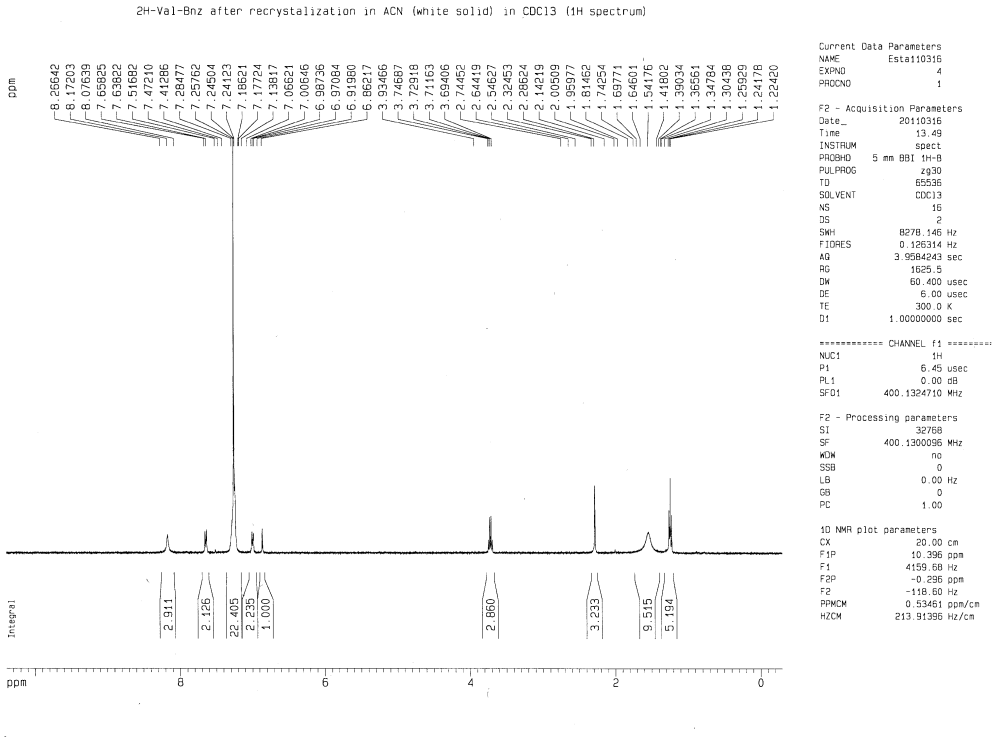

Figure S5. ^{1}H-NMR spectrum (400 MHz, 22 °C) in $CDCl_3$ of D-2,3,4,4,4,4',4',4'-[^{2}H]$_8$-valine benzyl ester.

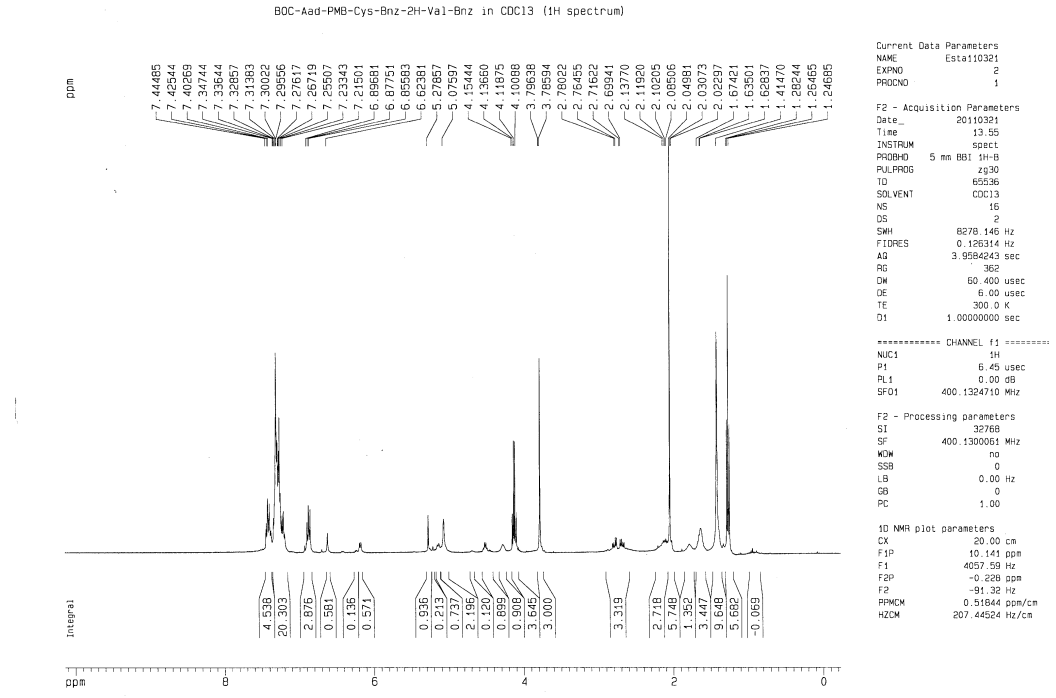

Figure S6. ^{1}H-NMR spectrum (400 MHz, 22 °C) in $CDCl_3$ of *N-tert*-butyloxycarbonyl-α-*p*-methoxybenzyl-δ-(L-α-aminoadipoyl)-*S*-benzhydryl-L-cysteine-D-2,3,4,4,4,4',4',4'-[^{2}H]$_8$-valine benzyl ester.

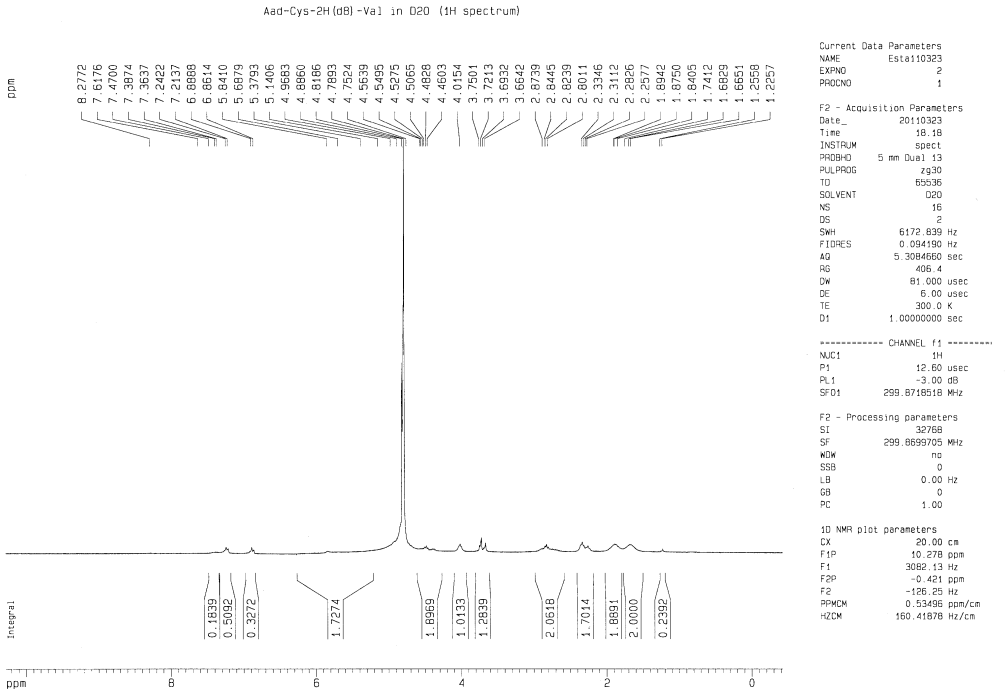

Figure S7. ^{1}H-NMR spectrum (300 MHz, 22 °C) in D_2O of δ-(L-α-aminoadipoyl)-L-cysteine-D-2,3,4,4,4,4',4',4'-[^{2}H]$_8$-valine.

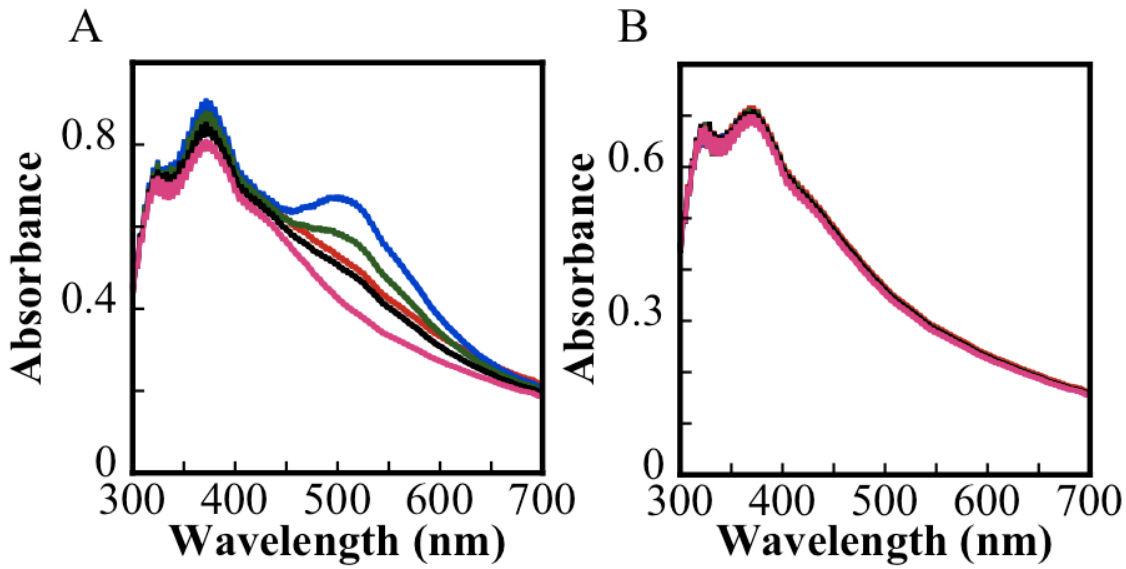

Figure S8. Absorption spectra from the reaction of the IPNS•Fe(II)•ACV complex with O_2. (**A**) Spectra acquired after 0.002 s (red), 0.020 s (blue), 0.10 s (green), 0.20 s (black), and 2.0 s (pink) after rapid mixing of a solution of the IPNS•Fe(II)•ACV complex (1.5 mM IPNS, 1.5 mM Fe(II), 0.5 mM ACV in 100 mM MOPS, pH 7.2) with an equal volume of oxygen-saturated buffer (at 5 °C, ~ 1.8 mM O_2). (**B**) Corresponding spectra from a matched control experiment lacking O_2,.

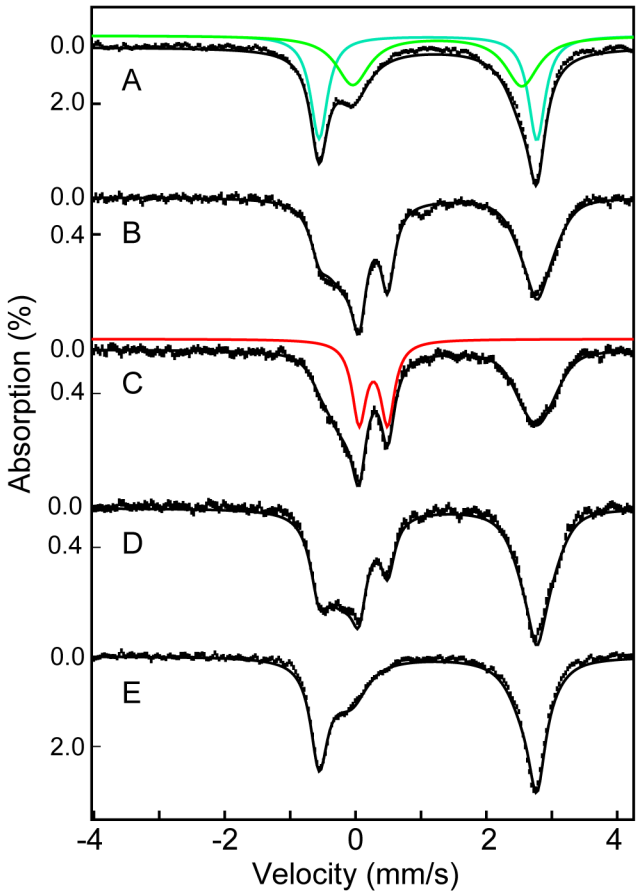

Figure S9. 4.2-K/zero-field Mössbauer spectra of freeze-quenched samples from the reaction of IPNS•Fe(II)•ACV with O_2. Reaction conditions were similar to those used in the SF-abs experiments (See Figure S10). Reaction times are indicated at the spectra. Spectrum of an O_2-free solution of the reactant IPNS•Fe(II)•ACV complex (1.8 mM IPNS, 1.8 mM Fe(II) and 20 mM ACV in 100 mM MOPS, 10% glycerol at pH 8.3, **A**) and spectra of samples prepared by mixing the reactant solution with two equivalent volumes of O_2-saturated (at 5 °C, giving ~ 1.8 mM O_2) buffer at 5 °C and freeze-quenching after 0.020 (**B**), 0.050 (**C**), 0.25 (**D**), or 60 s (**D**) are shown as vertical bars. The solid green, turquoise, and red lines are quadrupole-doublet simulations matching the spectra of the IPNS•Fe(II) and IPNS•Fe(II)•ACV complexes and Fe(IV)-oxo intermediate, respectively, according to parameters given in the text. A quadrupole doublet representing the IPNS•Fe(II)•IPN product complex, albeit with parameters different from those quoted in the main text (δ = 1.29 mm/s and $|\Delta E_Q|$ = 3.06 mm/s), was also used to fit the spectra.

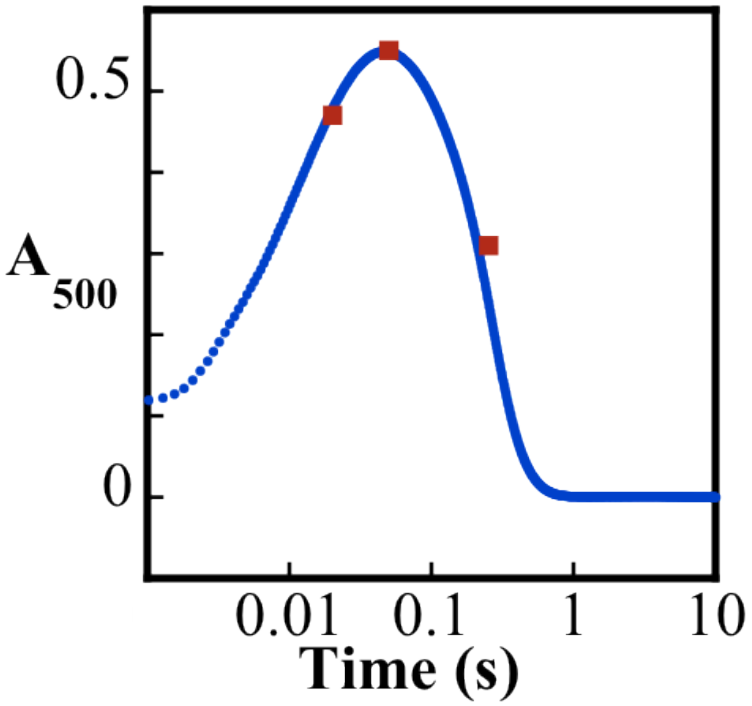

Figure S10. Comparison of the kinetics of absorbance at 515 nm determined in the SF-abs experiments (blue points) with the quantity of Fe(IV) intermediate determined in the FQ Mössbauer experiments (red points) performed under similar conditions. Final reaction conditions in the SF-abs experiment were 0.75 mM IPNS, 0.6 mM Fe(II), 10 mM ACV, and 0.6 mM O_2 in 100 mM MOPS, 10% glycerol at pH 7.2. In the FQ Mössbauer experiments, the only difference was that the final ACV concentration was 6.7 mM. Matching the blue and red points was achieved by assuming a molar absorptivity of the intermediate at 515 nm (ε_{515}) of 2.54 $mM^{-1}cm^{-1}$.

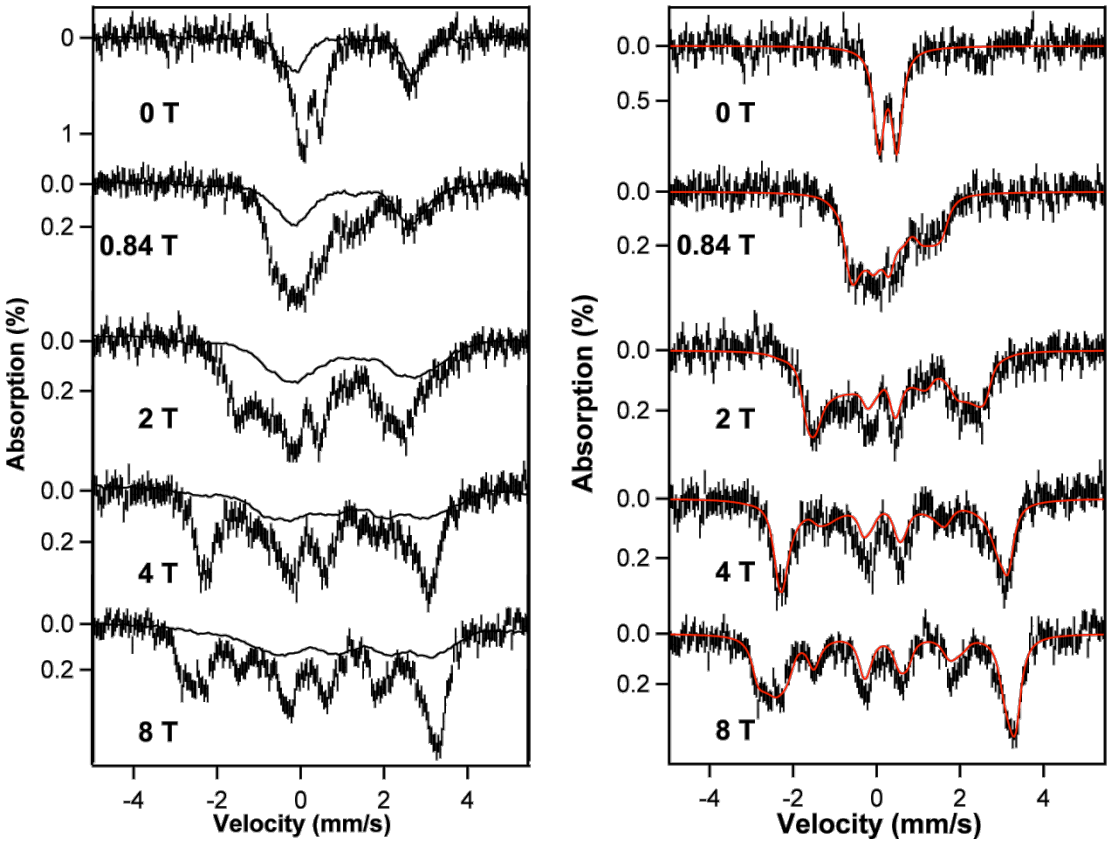

Figure S11. Left panel: Generation of the 4.2-K/variable-field Mössbauer reference spectra of the Fe(IV)-oxo complex in IPNS. Spectra of a sample generated by mixing at 5 °C of a solution of the IPNS•Fe(II)•ACV complex (conditions) with two equivalent volumes of O_2-saturated buffer and freeze-quenching after 0.050 s. The reaction conditions after mixing were 1.50 mM IPNS, 1.2 mM Fe(II), 8.3 mM ACV, and 1.2 mM O_2 in 100 mM MOPS, 10% glycerol at pH 8.3. Experimental spectra are shown as vertical bars. Spectra of a sample of the O_2-free IPNS•Fe(II) complex are shown as solid lines and are scaled to its amount in the 0.050-s sample (35 % of total intensity; determined from the zero-field spectrum). Removal of this spectral contribution yields the reference spectra of the Fe(IV)-oxo complex shown in the right panel as vertical bars. Red lines are spin-Hamiltonian simulations based on the assumption of an S = 2 electron-spin ground state and g = 2.0, D = 10 cm^{-1}, E/D = 0.09, δ = 0.28 mm/s, ΔE_Q = -0.43 mm/s, η = 1.5, $\mathbf{A}/g_n\beta_n$ = (-23.7, -17.8, -41) MHz, and Γ = 0.35 mm/s.

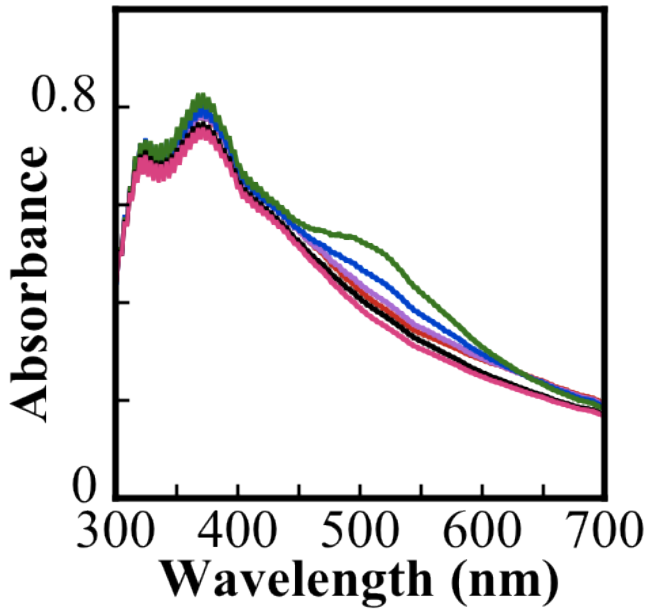

Figure S12. Raw SF-abs spectra from the reaction of the IPNS•Fe(II)•A[d_2-C]V with O_2. The spectra were acquired 0.002 (red), 0.007 (purple), 0.020 (blue), 0.10 (green), 0.50 (black), and 2.0 s (pink) after mixing of a solution containing 1.5 mM IPNS, 1.5 mM Fe(II), and 0.5 mM A[d_2-C]V in 100 mM MOPS, pH 7.2 with an equal volume of an O_2-saturated buffer solution (at 5 °C, giving ~ 1.8 mM O_2).

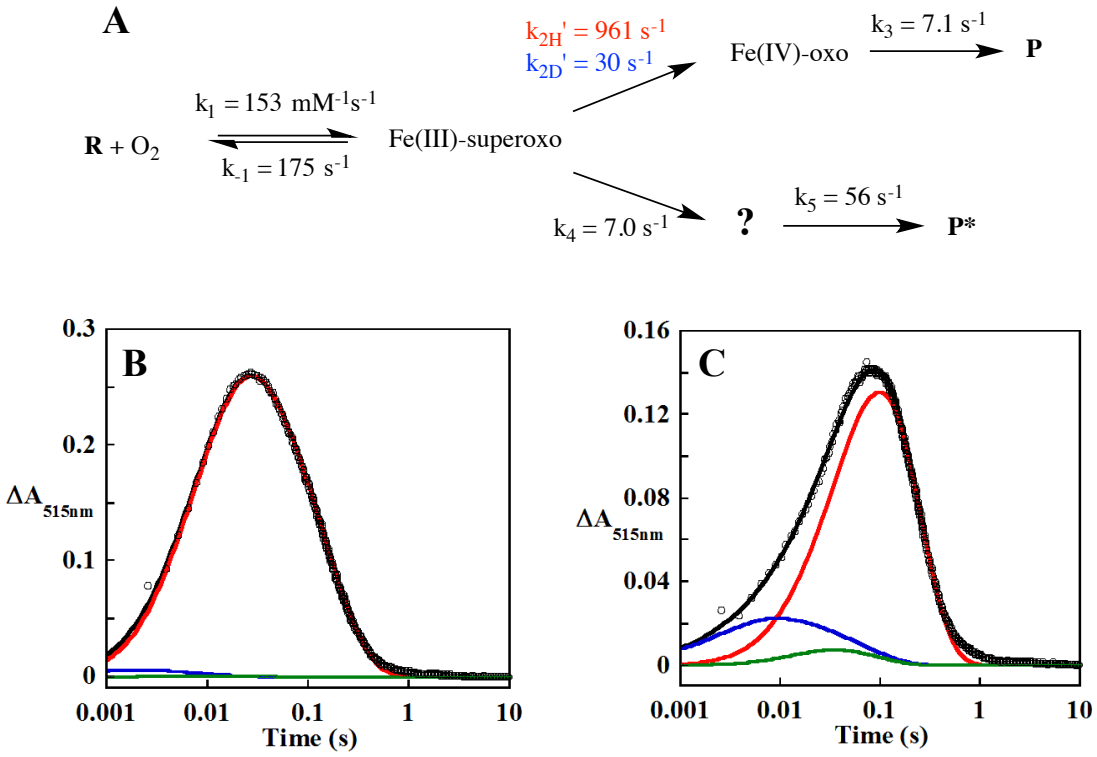

Figure S13. Alternative kinetic analysis of the reaction of the IPNS•Fe(II)•ACV/A[d_2C]V complex with O_2 at 5°C. Detailed experimental conditions are given in the legend of Figure 4. (**A**) A kinetic model modified from Eq. 3 of the main text to include the unproductive decay of the Fe(III)-superoxo intermediate to a transient off-pathway species, denoted as "**?**" that contributes to the absorption at 515 nm. The open black circles in panels (**B**) and (**C**) are the ΔA_{515}–vs-time kinetic traces for the reactions with unlabeled ACV and A[d_2-C]V, respectively. The black solid lines are simulations using the kinetic parameters shown in panel (**A**), where the blue, red and green lines demonstrate the individual contributions from the Fe(III)-superoxo, Fe(IV)-oxo intermediates, and the off-pathway species "**?**" to the absorption at 515 nm, respectively with molar absorption coefficients of 0.55 $mM^{-1}cm^{-1}$ for the Fe(III)-superoxo, 2.7 $mM^{-1}cm^{-1}$ for the Fe(IV)-oxo, and 2.1 $mM^{-1}cm^{-1}$ for the off-pathway species "**?**", respectively.

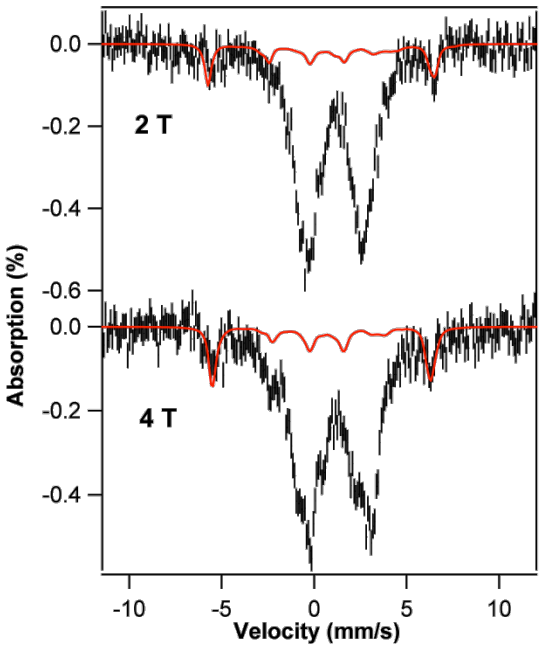

Figure S14. 4.2-K/variable-field Mössbauer spectra of the 0.010-s FQ Mössbauer sample generated by mixing the IPNS•Fe(II)•A[d_2-C]V complex with O_2-saturated buffer, as described in the main manuscript. The red solid lines are spin-Hamiltonian simulations matching the spectrum of the Fe^{III}-superoxo intermediate. For the simulation, the Hamiltonian given in Equation 4 of the main manuscript was expanded for the terms describing the exchange coupling interaction between the two electron spins, $\hat{\mathbf{H}}_{ex} = J_{iso}\cdot\mathbf{S_{Fe}}\bullet\mathbf{S_{SO}}$, and the electron Zeeman effect of the superoxide anion, which is assumed to be isotropic, $\hat{\mathbf{H}}_{Zeeman,SO} = g_{SO,iso}\cdot\mathbf{S_{SO}}\bullet\mathbf{B}$. The simulation parameters are: $S_{Fe} = 5/2$, $S_{SO} = 1/2$, $J_{iso} = 6$ cm^{-1}, $D_{Fe} = 0.5$ cm^{-1}, $(E/D)_{Fe} = 0.1$, $g_{Fe,iso} = 2.0$, $g_{SO,iso} = 2.0$, $A_{Fe,iso}/g_n\beta_n = -17.3$ T, $\Delta E_Q = 1.02$ mm/s, $\eta = 0$, $\delta = 0.53$ mm/s, and $\Gamma = 0.26$ mm/s (13 % of total intensity). We note that the values of δ and ΔE_Q were fixed to those determined from the analysis of the zero-field and low-field spectra, while the remaining parameters are similar to those observed experimentally for the Fe(III)-superoxo intermediate of HPCD.[11] We note that the parameters of the Fe(III)-superoxo intermediate in IPNS have not been uniquely determined.

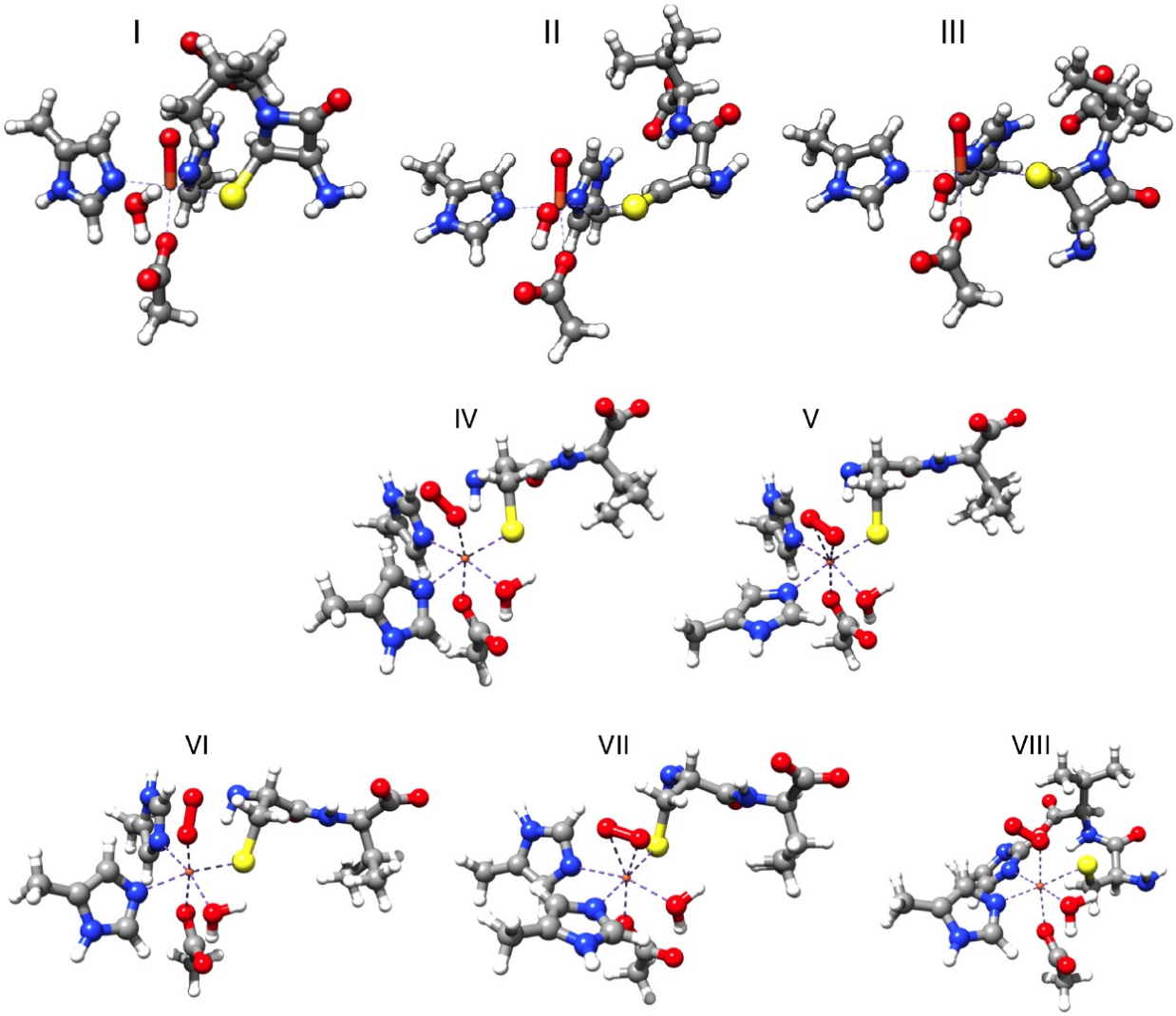

Figure S15. Possible structures of the Fe(IV)-oxo (I - III) and Fe(III)-superoxo (IV – VIII) intermediates calculated by density functional theory.

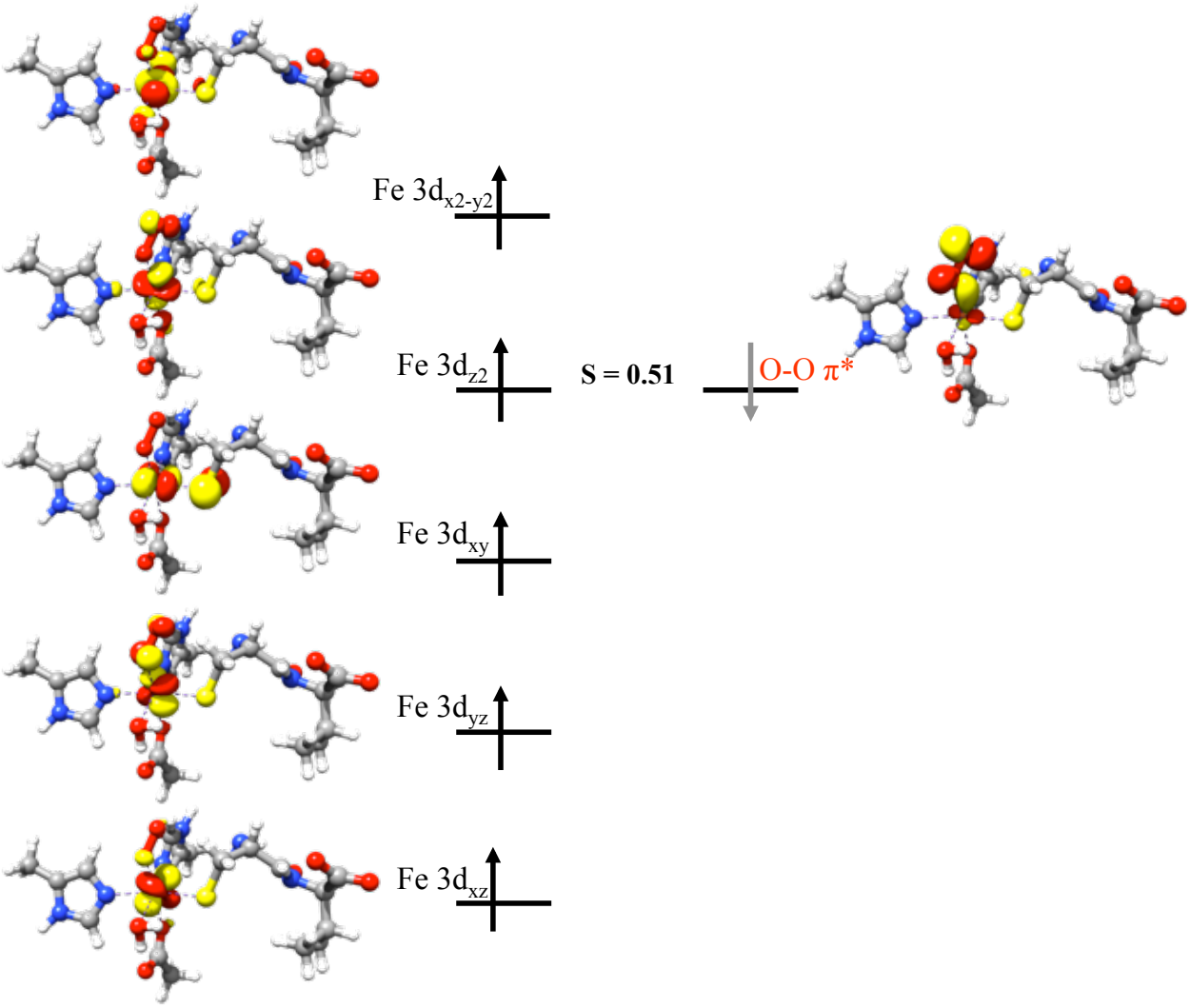

Figure S16. Molecular orbital diagram of model VI of the Fe(III)-superoxo intermediate.

Table S1. Relative quantities (in %) of the different IPNS complexes contained in samples prepared by reacting the IPNS•Fe(II)•ACV complex with O_2 and freeze-quenching at the indicated reaction times. The values were determined from analysis of the Mössbauer spectra, as described in the main manuscript.

Reaction time	0 s	0.020 s	0.12 s	0.45 s	90 s
IPNS•Fe(II)	65	10	19	47	45
IPNS•Fe(II)•ACV	35	35	35	35	35
Fe(IV)-oxo intermediate	0	28	21	5	< 2
IPNS•Fe(II)•IPN	0	27	25	10	18

Table S2. Relative quantities (in %) of the different IPNS complexes contained in samples, in which the IPNS•Fe(II)•A[d_2-C]V was reacted with O_2 for varying times. The values were determined from analysis of the Mössbauer spectra as described in the main manuscript.

	0 s	0.010 s	0.050 s	0.13 s	130 s
IPNS•Fe(II)	59	23	16	15	56
IPNS•Fe(II)•ACV	41	41	41	41	41
Fe(IV)-oxo intermediate	0	12	21	20	0
Fe(III)-superoxo intermediate	0	14	9	4	0
IPNS•Fe(II)•IPN	0	10	13	20	< 4

References

(1) Baldwin, J. E.; Schofield, C. J. In *The chemistry of β-lactams*; Page, M. I., Ed.; Blackie: London, 1991, p 1.

(2) Grummit, A. R.; Rutledge, P. J.; Clifton, I. J.; Baldwin, J. E. *Biochem. J.* **2004**, *382*, 659.

(3) Reimlinger, H. *Chem. Ber.* **1964**, *97*, 3493.

(4) Gill, S. C.; von Hippel, P. H. *Anal. Biochem.* **1989**, *182*, 319.

(5) Neese, F. *J. Inorg. Biochem.* **2006**, *100*, 716.

(6) Sinnecker, S.; Svensen, N.; Barr, E. W.; Ye, S.; Bollinger, J. M., Jr.; Neese, F.; Krebs, C. *J. Am. Chem. Soc.* **2007**, *129*, 6168.

(7) Price, J. C.; Barr, E. W.; Tirupati, B.; Bollinger, J. M., Jr.; Krebs, C. *Biochemistry* **2003**, *42*, 7497.

(8) Krebs, C.; Price, J. C.; Baldwin, J.; Saleh, L.; Green, M. T.; Bollinger, J. M., Jr. *Inorg. Chem.* **2005**, *44*, 742.

(9) England, J.; Martinho, M.; Farquhar, E. R.; Frisch, J. R.; Bominaar, E. L.; Münck, E.; Que, L., Jr. *Angew. Chem. Int. Ed.* **2009**, *48*, 3622.

(10) Krebs, C.; Galonić Fujimori, D.; Walsh, C. T.; Bollinger, J. M., Jr. *Acc. Chem. Res.* **2007**, *40*, 484.

(11) Mbughuni, M. M.; Chakrabarti, M.; Hayden, J. A.; Bominaar, E. L.; Hendrich, M. P.; Münck, E.; Lipscomb, J. D. *Proc. Natl. Acad. Sci., U.S.A.* **2010**, *107*, 16788.